Direct dynamic readout of molecular chirality with autonomous enzyme driven swimmers

Serena Arnaboldi, Gerardo Salinas, Aleksandar Karajić, Patrick Garrigue, Tiziana Benincori, Giorgia Bonetti, Roberto Cirilli, Sabrina Bichon, Sébastien Gounel, Nicolas Mano, et al.

Direct dynamic readout of molecular chirality with autonomous enzyme driven swimmers

Serena Arnaboldi[1†], Gerardo Salinas[1†], Aleksandar Karajić[1,2], Patrick Garrigue[1], Tiziana Benincori[3], Giorgia Bonetti[3], Roberto Cirilli[4], Sabrina Bichon[2], Sébastien Gounel[2], Nicolas Mano[2], Alexander Kuhn[1]*

[1] Univ. Bordeaux, CNRS UMR 5255, Bordeaux INP, ENSCBP, 16 avenue Pey Berland, 33607 Pessac, France, kuhn@enscbp.fr

[2] Centre de Recherche Paul Pascal, CNRS UMR5031, Univ. Bordeaux, Avenue Albert Schweitzer, 33600 Pessac, France

[3] Univ.degli Studi dell'Insubria, Dip. di Scienza e Alta Tecnologia,Via Valleggio 11, 22100 Como, Italy

[4] Centro Nazionale per il Controllo e la Valutazione dei Farmaci, Istituto Superiore di Sanità, Viale Regina Elena 299, 00161 Roma, Italy

†These authors contributed equally

Abstract

A key approach for designing bioinspired machines is to transfer concepts from nature to manmade structures by integrating biomolecules into artificial mechanical systems. This allows the conversion of molecular information into macroscopic action. In the present contribution, we describe the design and dynamic behavior of hybrid bioelectrochemical swimmers, which move spontaneously at the air/water interface. Their motion is governed by the diastereomeric interactions between immobilized enantiopure oligomers and the antipodes of a chiral probe molecule present in solution. These dynamic systems are able to convert chiral information present at the molecular level into enantiospecific macroscopic trajectories. Depending on the enantiomer in solution, the swimmers will move clockwise or anti-clockwise and the concept can also be used for the direct visualization of the degree of enantiomeric excess by analyzing the curvature of the trajectories.

Self-propelled artificial chemical swimmers are devices able to perform different complex tasks,[1,2] such as sensing[3-6] and cargo delivery,[6,7] while they move in fluids. Since 2002, when the first artificial autonomous swimmers were developed at the centimeter scale,[8] scientists aim to miniaturize such systems,[9] understand the mechanisms of motion, and achieve accurate motion control by taking inspiration from biomotors.[10] Examples of highly efficient biological motors include bacterial flagella,[11-12] spermatozoids,[13] motor proteins of the kinesin and dynein families, or F1-ATPase.[14]

An increasingly explored approach is the design of bioinspired machines by transferring biotechnological ingredients from nature to manmade structures.[9,15-17] A prominent example of such hybrid systems, combining biological components with synthetic ones, are enzyme-driven swimmers.[18-23] The enzymes can be coupled with artificial components to trigger more or less complex motion or rotation of micro-and nanodevices. For example, Soong *et al.* coupled F_1-ATPase to a Ni wire, which rotates when Na_2ATP is added.[24] Mano and Heller combined glucose oxidase and bilirubin oxidase on carbon fibers to generate macroscopic motion at the water-air interface,[25] whereas Feringa's group immobilized glucose oxidase and catalase on the surface of carbon nanotubes to power autonomous movement of the tubes in the presence of glucose.[26] Sanchez *et al*. integrated catalase also into microtubes to generate oxygen bubbles from hydrogen peroxide, leading to motion at low concentrations of fuel.[27] Other approaches involved the use of the same enzyme, both, with template-based microjets and Janus particles.[28-29]

Such hybrid machines can be used, among others, for the development of chemical sensors in which the swimming properties, such as speed, acceleration or motion direction, can be transformed into an analytically useful signal. Although chemical sensing through bioinspired micro-and nanoswimmers is still at an early stage, these systems present different advantages compared to common electrochemical or optical sensors, among which one can mention

sensitivity, immunity to electrical interferences and, most importantly, operation in a wireless manner.[10]

Different approaches in the literature are focusing on the correlation between the swimmer properties and the concentration of an analyte in solution,[30] such as heavy metals,[28,31] amino acids,[10] or other organic compounds.[32] In addition, these systems can be used to mimic the behavior of microorganisms in the presence of chemical gradients (chemotaxis).[10] In the frame of these contemporary analytical challenges, one important aspect is the qualitative and quantitative detection of chiral molecules. However, designing hybrid swimmers, capable of translating chiral molecular information into macroscopic motion has not been reported so far. The few examples present in the literature, which combine chiral information and swimmer systems, are based *e.g.* on photoinduced phenomena in which light is converted into helical motion[33] or where polarized light is used for out-of-plane deformations of polymer films.[34]

In this context, we report here a hybrid bioelectrochemical swimmer whose trajectory is intimately related to the chirality of molecules present in solution. We propose a system combining three different ingredients: *i)* polypyrrole (Ppy) as the basis of the swimmer architecture, with good mechanically and electric properties, *ii)* an enzyme (bilirubin oxidase, BOD) providing the driving force of the swimmer motion, and *iii)* an inherently chiral oligothiophene ensuring high enantioselectivity towards the antipodes of chiral analytes. The latter component has already been employed as an enantiospecific selector when present on electrode surfaces,[35] in particular on polypyrrole films.[36]

The synergy of these three ingredients allows designing an original hybrid device, coupling the capability of BOD enzyme to reduce oxygen with the enantioselective oxidation of chiral probe molecules by the inherently chiral oligomers. Both compounds are immobilized on the surface of a miniaturized Ppy strip to allow electron transfer between reduction and oxidation sites. The

resulting, charge compensating, asymmetric proton flux along the swimmer [37] induces an enantiospecific macroscopic circular motion. Consequently, the swimmer trajectory is clockwise or anti-clockwise, as a function of the enantiomer present in solution, and the curvature of the track can be used as a direct readout of enantiomeric excess.

Results

The hybrid swimmers were designed according to Figure 1. First, a Ppy layer is deposited on a gold-plated glass slide, according to a procedure described in previous work.[38-40] Then Ppy is peeled off from the electrode, and cut to obtain a rectangular film of approximately 5 mm length, which is divided into two strips until the middle of the rectangle (right side of Figure 1 C). The inherently chiral monomers, enantiopure (*R*)- or (*S*)-2,2′-bis[2-(5,2′-bithienyl)]-3,3′-bithianaphthene, ((*R*)-BT_2T_4 and (*S*)-BT_2T_4) (Figure 1 A), are then electrodeposited separately on these two strips. A hydrogel, composed of an osmium polymer (the redox mediator, Med), crosslinker and BOD enzyme, is then drop casted on the opposite extremity of the object and left overnight in a fridge (details in the Supplementary Information). In this way, the BOD enzyme is entrapped in the redox hydrogel, which acts not only as an immobilization matrix, but simultaneously also as a redox mediator. This allows ensuring mediated electron transfer, which is much more efficient than direct electron transfer, and increasing the amount of immobilized enzyme, compared to what would be possible by direct grafting via a chemical bond or by physisorption of a monolayer.

In order to verify the enantiodiscrimination ability of the BT_2T_4 oligomers deposited on the surface of the freestanding Ppy strip, differential pulse voltammetry (DPV) was performed in the presence of L- or D-3,4-dihydroxyphenylalanine (L- or D-DOPA) in a citrate/phosphate buffer solution at pH 5. Figure 2 A and B illustrate the pronounced enantioselectivity of the

BT_2T_4 oligomers electrodeposited as enantiopure antipodes on the Ppy strips. In the case of the (*S*)-BT_2T_4 oligomer, a peak-to-peak separation of 600 mV between the two signals recorded with L-DOPA and D-DOPA is observed (Figure 2A). An analog result is obtained when inverting the oligomer configuration (Figure 2 B). As this potential difference between the DOPA isomers is very high, it is possible to assume that the two strips of the designed hybrid film are able to selectively oxidize L- or D-DOPA without crosstalk.

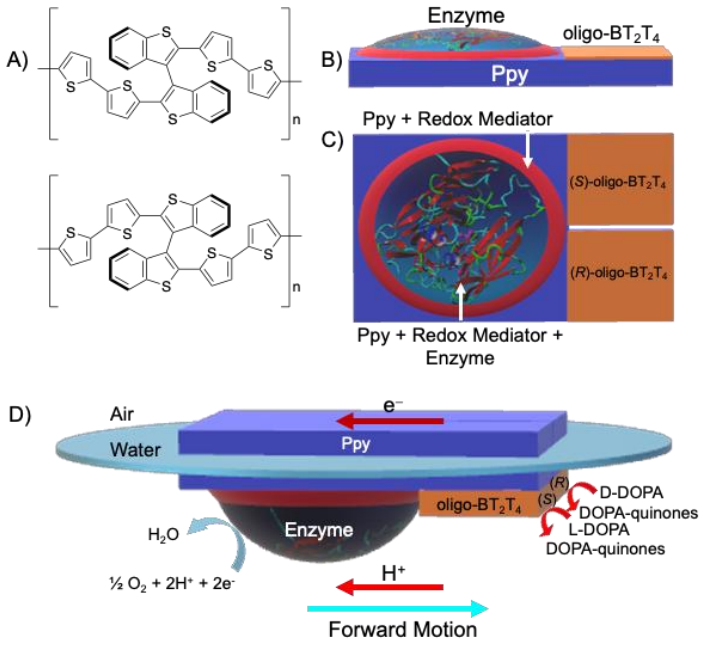

Figure 1. **Design of the enantiosensitive swimmer.** A) Chemical structures of the BT_2T_4 enantiopure oligomers, used for the electrodeposition on the Ppy surface to induce right or left-handed motion. B) Side view of the hybrid swimmer. The enzyme, together with the redox polymer ($Med_{ox/red}$) and the crosslinker, is drop-casted on top of the Ppy film at the left side. The thin layer of enantiopure BT_2T_4 oligomer electrodeposited on Ppy is depicted on the right side. C) Top view of the swimmer illustrated in (B). Both enantiopure oligomers are visible on the right side localized at the surface of the individual Ppy arms. The cut between these two strips allows electrodepositing separately the two enantiopure antipodes. D) 3D illustration of the swimmer in an upside-down configuration at the air/water interface together with a representation of the mechanism of selective motion induced by proton flux. Two different reactions occur at each extremity of the swimmer, reduction of oxygen and the selective oxidation of either L- or D-DOPA, depending on the composition of the solution.

Consequently, if only one of the two DOPA probes is present in solution, the oxidation will preferentially take place at only one of the oligomer-modified strips. This oxidation is coupled with a reduction reaction, which needs to occur at a more negative formal potential, thus providing the thermodynamic driving force for a spontaneous overall reaction. This reduction is achieved *via* the conversion of oxygen to water by BOD[41] at the opposite extremity, and the electrons are shuttled from the oligomer-modified part to the enzyme *via* the conducting polymer substrate.

When this hybrid object is placed upside-down at the air/water interface of a solution (Figure 1D), containing one or the other enantiomer of a chiral analyte (in the present work L- or D-DOPA), a clockwise or anticlockwise motion is respectively observed. This can be explained by the fact that the electron flow from the oligomer-modified extremity to the enzyme-modified section has to be accompanied by a proton flux along the specific edge of the swimmer strip, which is modified with the oligomer having the chirality matching with the probe present in solution. Such motion of protons relative to the swimmer can be achieved either by moving liquid along one side of the object or by moving the object itself, depending on the motility of the object. This phenomenon, also known as self-electrophoresis,[42-44] has been already used intensively for designing different types of micro- or nanoswimmers,[45-46] as well as autonomous pump systems.[37,47] In the present case, as the swimmer is very mobile, it will start moving at the air-water interface, with the driving force being generated preferentially along only one edge of the polymer film, and the resulting torque force induces a curved trajectory. Figure 2 C illustrates the movement of a swimmer in contact with a 5 mM D-DOPA solution. Motion is in this case clockwise, since the oxidation reaction occurs only on the part of the object modified with (*R*)-BT_2T_4 oligomer.

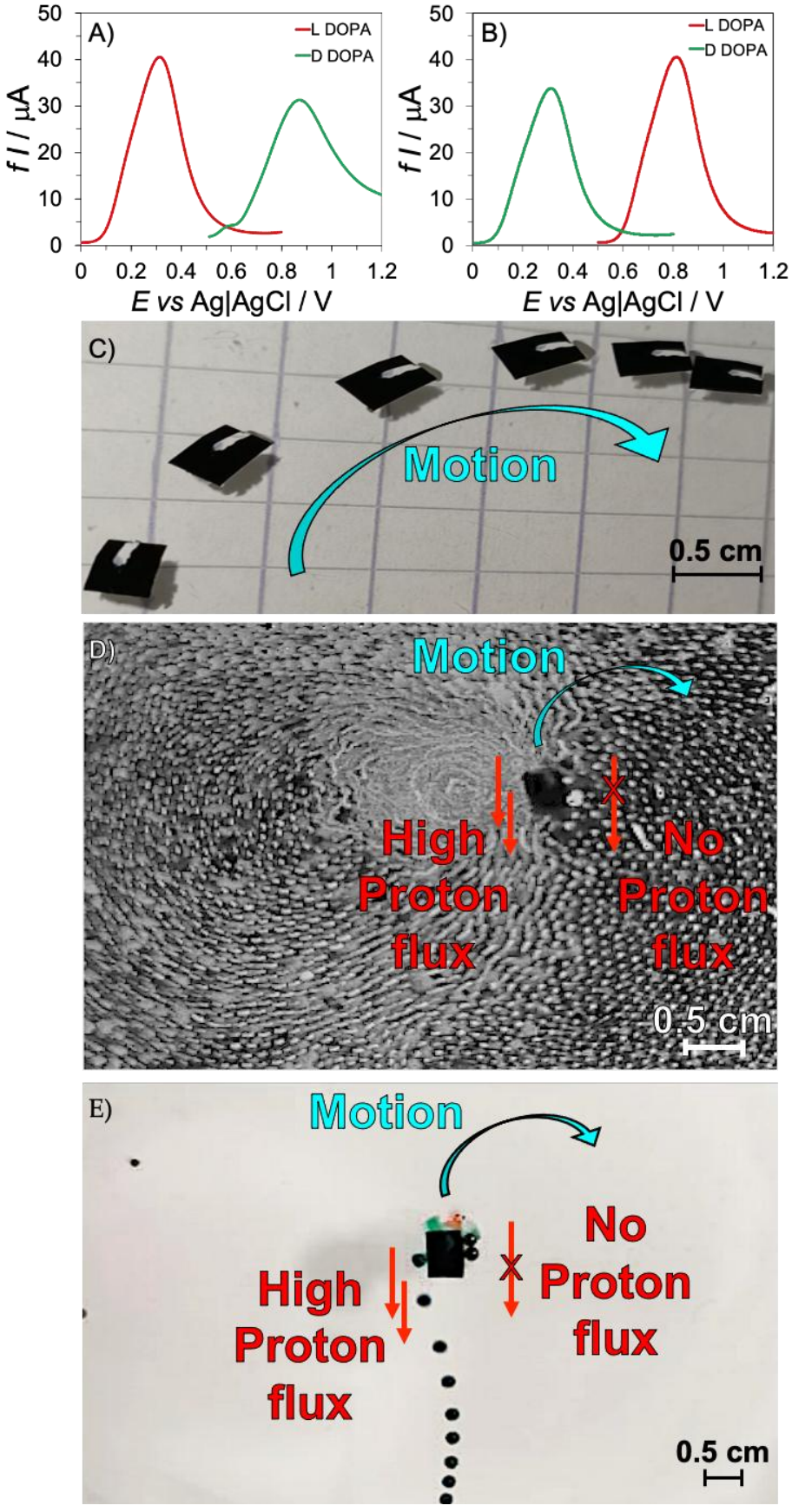
A)
L DOPA
D DOPA
f I / µA
E vs Ag|AgCl / V
B)
L DOPA
D DOPA
f I / µA
E vs Ag|AgCl / V
C)
Motion
0.5 cm
D)
Motion
High Proton flux
No Proton flux
0.5 cm
E)
Motion
High Proton flux
No Proton flux
0.5 cm

Figure 2. Mechanism responsible for the enantiosensitive motion. A) Differential pulse voltammetry signals of the enantioselective electrooxidation of 5 mM L- or D-DOPA in water and 0.1 M $LiClO_4$ recorded with a hybrid polymer layer composed of either Ppy + oligo-(*S*)-BT_2T_4 or B) Ppy + oligo-(*R*)-BT_2T_4. C) Video frames of the clockwise motion captured at different times when the swimmer is placed in a 5 mM D-DOPA solution. The cut between the two oligomer-modified segments is highlighted in white. D) Illustration of the hydrodynamic flow around the Ppy swimmer in an experiment where the swimmer is immobilized on a support. The two enantiopure oligomer modified strips, constituting the anode, are pointing upwards, and the enzyme-covered part is oriented downwards. The swimmer is placed in a 5 mM D-DOPA 0.3 M citrate/phosphate buffer (pH 5) at 22°C, containing a large concentration of 1mm carbon beads E) Same experiment as in (D) but with only a small amount of carbon beads acting as individual tracers of the hydrodynamic flow.

The hybrid swimmer can be considered as an intrinsically bipolar object, formed by an anode and a cathode, one releasing protons and the other one consuming protons according to the following reactions:

$DOPA \rightarrow DOPA_{quinone} + 2\ e^- + 2\ H^+$ (anode)

$\frac{1}{2}\ O_2 + 2\ H^+ + 2e^- \xrightarrow{BOD} H_2O$ (cathode)

$Med_{ox} + e^- \leftrightarrows Med_{red}$ (cathode)

At the enzyme side, the BOD inside the hydrogel reacts through a mediated electron transfer, reducing oxygen at the water-air interface,[48] whereas at the opposite extremity, a DOPA enantiomer is transformed into its oxidized quinone analog. These coupled reactions generate a strong proton flux, which can be easily visualized if the swimmer is on purpose immobilized at a fixed position. In this case, only the liquid can move and the resulting hydrodynamic flow can be tracked by adding carbon beads to the solution. Figure 2 D clearly illustrates the asymmetric flow pattern, driven by the proton flux from the anode to the cathode, eventually leading to a vortex of carbon beads at the active edge of the swimmer, whereas at the opposite inactive edge no motion of beads is detected (Supplementary Video S1). In this particular experiment, D-DOPA was present in solution and therefore it can be only oxidized at the part of the

hybrid object where the (*R*)-oligomer is immobilized (left arm of the strip), coupled with the simultaneous oxygen reduction by BOD. Thus, on the left edge of the swimmer, carbon beads are ejected towards the backside, whereas at the right side the tracking particles remain immobile.

A similar behavior is observed when repeating the same experiment with a smaller amount of carbon beads. In particular, we performed two different tests. In the first one, only a single carbon bead was placed on one edge of the swimmer (Figure 2 E and Supplementary Video S2). The other experiment was carried out by placing along the left edge of the swimmer several carbon beads (Supplementary Figure S1 and Supplementary Video S3).

In order to further confirm that self-electrophoresis is the underlying mechanism, we have performed the same experiment as described above and depicted in Figure 2C, but in solutions with different ionic strength: 0.15 M, 0.3 M and 0.5 M. We observed that swimmers have a higher speed in the 0.15 M buffer solution (Video S4). In contrast to this, swimmers are much slower in a 0.5 M solution (Video S5). The measured average speeds were 6.4 cm s^{-1} and 0.4 cm s^{-1}, respectively, indicating that with such an increase in ionic strength of the solution the speed decreases by about 90% (Figure S2). In parallel, we have also performed electrochemical measurements of the turnover of the enzyme under the same conditions to verify whether the change in speed might be partially related to a change of the enzyme activity as a function of ionic strength (Figure S3). We observed that the enzyme electrocatalysis is only slightly affected by the change in ionic strength within standard errors (15-20%). Thus, the change in speed is essentially related to a decrease in self-electrophoresis efficiency when increasing the ionic strength of the solution. A total quenching of self-electrophoresis occurs only at significantly higher concentrations than the ones used in our study, leading for example to a complete suppression of the swimmer motion in 1M buffer solution.

Figure 3 summarizes all the possible macroscopic enantioselective trajectories of the hybrid swimmers in a 0.3 M buffer citrate/phosphate solution (pH 5) at 22°C containing A) 5 mM of D-DOPA or B) 5 mM of L-DOPA, or D) a racemate of the two probes (10 mM total concentration). When (*R*)-oligomer is deposited on the left strip of Ppy and the (*S*)-oligomer on the right, motion is clockwise in the presence of D-DOPA in solution (Figure 3 A, Supplementary Video S6). On the contrary, when L-DOPA is in solution, the motion of a hybrid swimmer with the same configuration is anticlockwise (Figure 3 B, Supplementary Video S7). A perfect control of the trajectory's curvature is possible, since it depends strongly on the configuration of the enantiopure oligomers deposited on the strips of the Ppy. In order to illustrate this point more clearly, two swimmers with opposite oligomer configuration were prepared and placed simultaneously in the same buffer solution containing only L-DOPA (Figure 3 C, Supplementary Video S8). In this case, motion is controlled by the position of the (*S*)-oligomer and its diastereomeric interactions with L-DOPA, the antipode which is preferentially transformed from a thermodynamic point of view. When the (*S*)-oligomer is present on the right arm of the swimmer (and the (*R*)-oligomer on the left arm), the swimmer spins anticlockwise, whereas for the opposite configuration the rotation is clockwise. Furthermore, when both swimmers (with opposite oligomer configuration) are placed at the surface of a racemic solution of the chiral probe, straight trajectories are obtained, because now both arms are equally redox-active, thus leading to a symmetric proton flux along the two edges of the Ppy film (Figure 3 D, Supplementary Video S9).

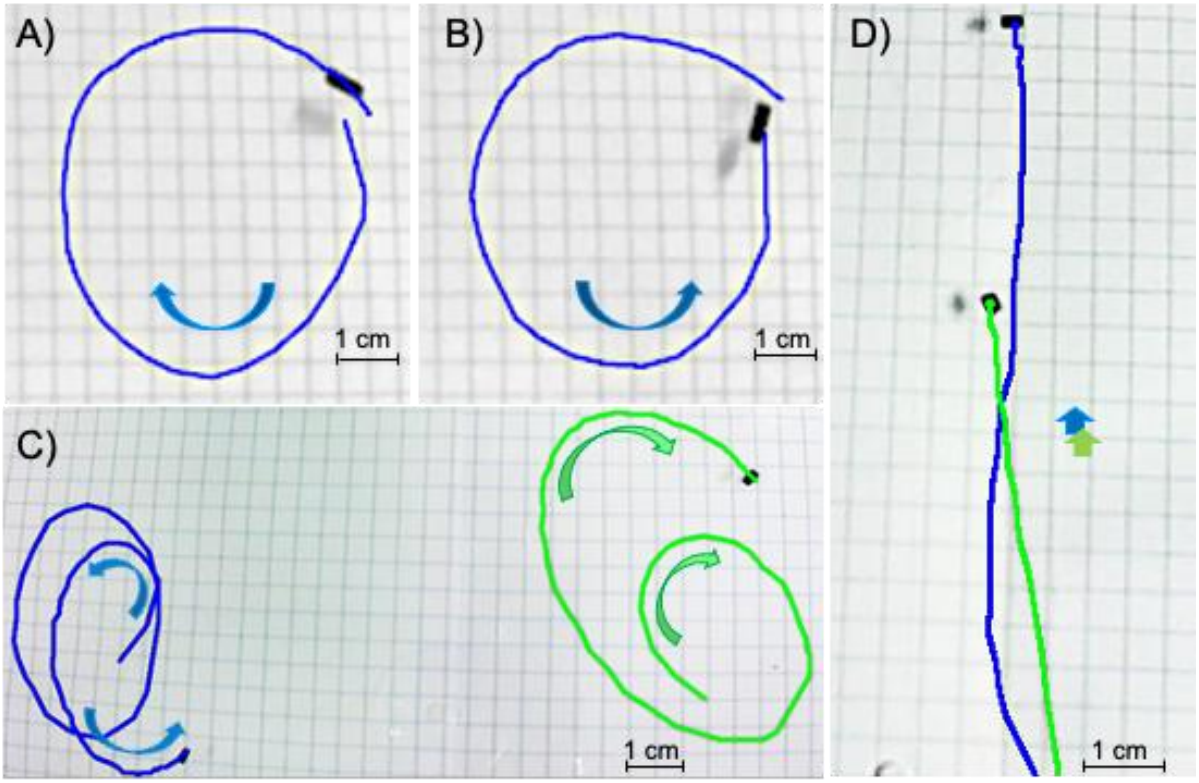

Figure 3. Characteristic swimmer trajectories. Macroscopic enantiospecific motion of swimmers placed at the air/water interface of a 0.3 M citrate/phosphate buffer (pH 5) at 22°C containing A) 5 mM D-DOPA, B) 5 mM of L-DOPA, C) 5 mM L-DOPA and D) a racemic mixture of L- and D-DOPA with a total fixed concentration of 10 mM. The swimmer on each figure represents its final position. The direction of the motion depends on the diastereomeric interactions between the probe in solution and the favored enantiopure oligomer deposited on the Ppy. In A) (*R*)-BT_2T_4 is deposited on the left arm of the strip and reacts preferentially with D-DOPA in solution so the motion is clockwise; the opposite is observed in the case of B) where L-DOPA in solution reacts with (*S*)-BT_2T_4 deposited on the right strip and the motion is anticlockwise. In C) the blue line corresponds to the track of a swimmer with the (*S*)-oligomer deposited on the right strip, the green one is related to a swimmer with the same oligomer deposited on the left strip. Both swimmers are launched simultaneously in the presence of L-DOPA. In D) the green trajectory is related to a swimmer with the (*R*)-BT_2T_4 oligomer deposited on the right arm and (*S*)-BT_2T_4 on the left arm, whereas the blue trajectory refers to an object with the opposite configuration. Both swimmers are launched simultaneously in the presence of a DOPA racemate. In A, B, D the swimmer is 8mm long and 4 mm in C.

The motion trajectories usually highly depend on the geometric parameters of the swimmers; for longer objects we have observed a decrease in the average speed. The swimmers shown in Figure 3A and 3B are two times longer (8 mm)

compared to the ones in Figure 3C (4 mm), while keeping all the other parameters constant. By calculating and comparing the speed values obtained from Video S6, S7 and S8, we can conclude that for the latter swimmers the average speed is 13 cm s^{-1}, instead of 5 cm s^{-1} for the 8 mm long swimmers, corresponding to approximately 30 and 6 body lengths per second, respectively. The average speed of the hybrid swimmers has also been studied as a function of the solution composition. In the presence of 5 mM of a single DOPA probe, the calculated average speed for the 8 mm long swimmer is 5 cm s^{-1}, whereas for the racemic solution, with a total concentration of 10 mM, the speed of the swimmers is around 9 cm s^{-1}. The reason is that in the latter case, proton flux is generated along both edges, and therefore the object experiences a higher driving force. This is the first indication that the speed of the hybrid swimmers strongly depends on the DOPA concentration in solution.

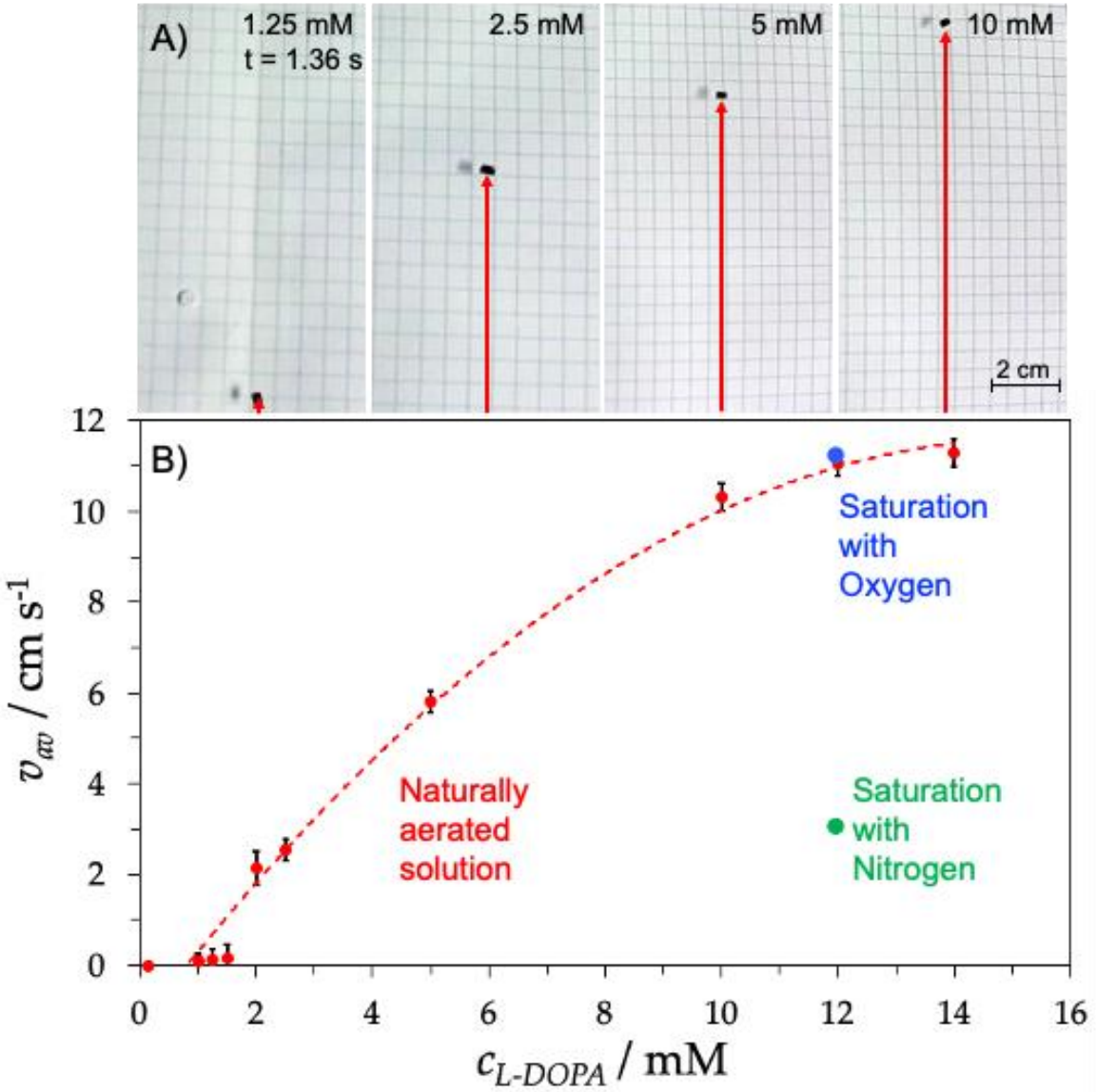

Figure 4. Quantitative analysis of the swimmer speed. Average speed values of swimmers as a function of L-DOPA concentration in the range from 0.15 mM to 14 mM, in a 0.3 M phosphate/citrate buffer solution at pH 5 at 22°C. The swimmer on each figure represents the final position at the end of each trajectory. For these experiments, instead of depositing the two oligomers on the respective arms of the swimmer, only (*S*)-BT_2T_4 oligomer is deposited on the entire extremity of the swimmer to generate linear motion. A) Final positions of the swimmers for different concentrations recorded after the same period of time (1.36 s). B) Calibration plot of swimmer speed as a function of L-DOPA concentration. Red dots represent the measures carried out in a naturally aerated solution, whereas the green dot is related to a measure carried out with 12 mM L-DOPA in a buffer solution saturated with nitrogen. The blue dot refers to a measure performed under the same conditions, but in a buffer solution saturated with oxygen. The error bars represent the average of three measurements.

In order to investigate this aspect in more detail, the swimmer speed was measured as a function of the L-DOPA concentration ranging from 0.15 mM to 14 mM. For these experiments, the design of the swimmer was slightly changed. Instead of having two arms, separated by a cut, and modified with the two enantiopure oligomers, (*S*)-BT_2T_4 was now deposited on the entire extremity without cutting the Ppy. This design was adopted to guarantee a perfect linear motion.

Figures 4 A and B illustrate the trend of the swimmer speed as a function of L-DOPA concentration. In particular, in Figure 4 A, the final positions of the objects are recorded at a fixed time for four different L-DOPA concentrations. Figure 4 B shows the resulting calibration curve, which can be assimilated to characteristic plots obtained for Michaelis Menten type kinetics. According to this model, for low substrate concentrations, the reaction speed increases in an almost linear way, whereas at higher concentrations, the enzymatic conversion becomes kinetically limited and a plateau is reached. Further additions of substrate aliquots do not change the speed of the swimmer. However, for too low concentrations (0.15 mM, 1.0 mM, 1.25 mM, 1.5 mM) the average speed is too small to be considered as significant with respect to the error bars. We found out that that the minimum concentration of L-DOPA that can induce a significant motion of the swimmer is 2 mM. This threshold concentration seems to be necessary to overcome friction forces related to the viscosity of the solution. In order to verify the Michaelis Menten type behavior and identify parameters, other than the DOPA concentration, which might affect the swimmer speed, additional experiments were carried out. All measurements represented by red dots in Figure 4 B were performed at room temperature and in a naturally aerated solution, where the concentration of O_2 is small due to its intrinsically low solubility. To check whether this low oxygen concentration is the rate-limiting factor in the high DOPA concentration regime, the speed of a swimmer was measured in the presence of 12 mM L-DOPA, but this time in an

oxygen saturated solution. No significant changes in speed were observed, indicated by the blue dot in Figure 4 B. Thus, the naturally present oxygen concentration is high enough and is not the rate-limiting factor, but the intrinsic turnover of the enzyme, as it can't ensure a sufficiently fast reduction reaction to consume the total flow of electrons liberated by the DOPA oxidation. To double-check that oxygen reduction is indeed involved in the reaction mechanism providing the driving force for the swimmer, a second experiment has been carried out with the same swimmer, but in a nitrogen saturated solution. Under these conditions, a drastic decrease in speed is observed (green dot in Figure 4 B). The remaining small speed is due to residual oxygen, which can't be completely removed by nitrogen bubbling or which slowly reenters the solution during the recording.

To verify that the proposed mechanism is not limited to the selective conversion of only one type of molecule, we explored the possibility to replace DOPA with another chiral analyte. In this context, we studied the motion of swimmers placed at the air/water interface of a 0.3 M buffer citrate/phosphate solution containing 0.25 mM L-ascorbic acid (L-AA). The diastereomeric interaction between the (*S*)-oligomer and L-AA is more favorable from a thermodynamic point of view, as we could verify again by DPV measurements (Figure S4). The obtained peak separation in this case is only around 100 mV, but nevertheless an enantioselective motion is observed (Video S10, S11). When the (S)-oligomer is present on the right arm of the object, the swimmer spins anticlockwise, whereas for the opposite configuration the rotation is clockwise. We can therefore conclude that the present concept is of general character. The swimmer shows an enantiospecific trajectory even if the energy difference between two enantiomers is less important (in this case 100 mV instead of 600 mV for DOPA). Another point worth underlining is that the approach even works with a probe that has a completely different chemical nature compared to DOPA, because ascorbic acid has not an aromatic structure.

A further very interesting aspect is the fact that the swimmers are not only able to move in buffer solution, but also in biological media such a serum. When bovine serum is spiked with 10 mM L-DOPA, a clockwise trajectory is observed, which is coherent with the favorable diastereomeric interaction between the (*S*)-BT_2T_4-oligomer deposited on the left arm of the swimmer and the L-DOPA probe in solution (Video S12). It is important to mention that serum has a very complex composition with a rather high ionic strength related to the high osmolality (typically 250-350 mOs l^{-1}) and a higher viscosity. This obviously can impact the intrinsic speed, but we were able to measure velocities that are comparable with the characteristic values observed for 0.5 M buffer solutions (0.5 cm s^{-1}).

The general lifetime of the swimmers was tested by repeating the experiment described in Figure 3 B. We have observed that after one or two rotation cycles the objects start to decelerate. This means that a given swimmer has only a limited lifetime. Stability is a general problem for enzyme-based bioelectrochemical devices, such as biosensors or biofuel cells. The instability can result from either a desorption/leakage from the surface, or a slow intrinsic deactivation of the enzyme itself. In the current case, and in contrast for example to biofuel cells, the enzyme layer, which is facing the solution, is experiencing rather strong hydrodynamic effects, as evidenced by the almost turbulent liquid flow shown in Figure 2D. Therefore, the hydrogel/enzyme layer might be gradually removed by the shear forces present along the surface.

To confirm this hypothesis, the same swimmer was tested again under the same experimental conditions, but after immobilizing again on the PPy a hydrogel containing a fresh aliquot of BOD, the redox polymer and the crosslinker. The swimmer started to move again with an average speed value of 5 cm s^{-1}, comparable to the one obtained previously under the same conditions (5 mM L-DOPA in buffer at pH 5) (Supplementary Video S13). The degradation of the swimmer in terms of active elements was also examined by scanning electron

microscopy (SEM) (Figures S5, S6) and energy-dispersive X-ray spectroscopy (EDS) (Figures S7, S8). Comparing a swimmer before and after performing the swimming experiments revealed that the oligo-BT_2T_4 side was not damaged during the continuous oxidation of the DOPA probe. However, the swimmer loses enzyme hydrogel, as confirmed by the EDS graphs, showing a decrease in copper concentration which is characteristic of the enzyme's active site. Altogether, those experiments indicate that leaching of the enzyme is the reason for the decrease in speed, but the layer could be stabilized, as for other bioelectrochemical devices, by adding a mechanically stronger protecting layer on top of the enzyme-containing hydrogel film.

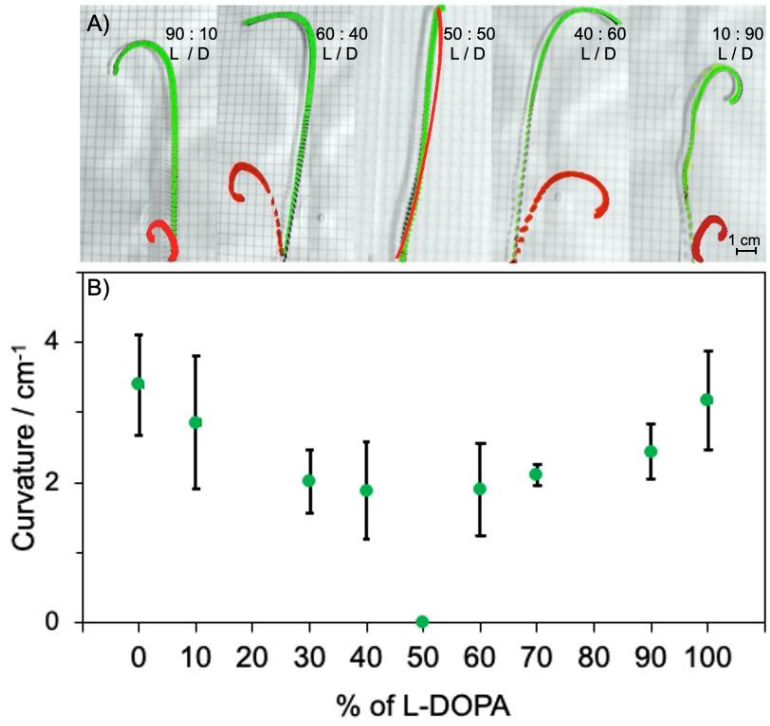

Figure 5. Monitoring of enantiomeric excess. A) Macroscopic enantiospecific motion of swimmers placed in 0.3 M citrate/phosphate buffer solutions at pH 5 at 22°C containing different enantiomeric ratios of DOPA probes. The different proportions of L-DOPA/D-DOPA from left to right are as indicated in the Figure: 90:10, 60:40, 50:50, 40:60, 10:90. The green trajectories correspond to a constant total concentration of L- + D-DOPA of 5 mM, the red trajectories correspond to a constant total concentration of L- + D-DOPA of 2.5 mM. B) Curvature values *vs* percentage of L-DOPA present in solution with a total concentration of L-DOPA + D-DOPA of 5 mM. The error bars represent the average of three measurements.

As the driving force for the motion is generated selectively at the individual oligomer modified Ppy arms, one can speculate that it should also be possible to use the curvature of the swimmer trajectory to get some information about the ratio between two chiral probes present in solution. Therefore, we studied the macroscopic motion of the hybrid swimmer in solutions containing different ratios of DOPA enantiomers. Figure 5 A illustrates the trajectories recorded in a 0.3 M citrate/phosphate buffer solution at pH 5 at 22°C, containing different ratios of the two molecular antipodes, with a constant total concentration of 5 mM (green) and 2.5 mM (red). The green trajectories typically present two segments, first a straight part with a similar average speed of around 4 cm s^{-1}, and a second part where the swimmers start to turn due to the specific selective interactions with L- and D-DOPA in solution. The difference in trajectories when comparing Figure 5 A and Figures 3 A, B and C, can be explained in terms of competition between the two enantioselective oxidation reactions. In the first part, both oligomers are equally redox active for the conversion of the chiral probes, thus the resulting trajectories are straight, similar to what has been observed in Figure 3 D. In the second period, after a partial local depletion of DOPA on both sides, the oxidation reaction with the DOPA enantiomer which is present at a higher concentration becomes predominant and therefore the object starts to turn clockwise or anticlockwise. This is caused by the formation of an asymmetric proton flux along both swimmer edges. This hypothesis is also confirmed by recording the trajectories at a lower total concentration, for which the local depletion effect occurs earlier (red lines in Figure 5 A). The average speed of the swimmers is in this case lower, in agreement with the correlation shown in Figure 4 B, and the objects start to turn almost immediately.

It is worth noticing that for the case of the green trajectories it is possible to plot the curvature of the second period, as a function of the relative amount of L-DOPA. A graph with mirror symmetry is obtained (Figure 5 B). This indicates

that the curvature directly reflects the enantiomeric excess in solution. The two oligomers selectively react with the enantiomeric DOPA probes in a specular way, allowing an easy estimation of this important analytical parameter. The slight difference between the two trends as well as the error bars are not due to an intrinsically different reactivity of the BT_2T_4-oligomers, but to small differences in the swimmer morphology. Another way to illustrate the correlation between the curvature of the trajectory and the enantiomeric excess is to plot the so-called straightness index. The latter is defined by the ratio between the direct distance (D), measured from the end to the starting point of the trajectory, and the total path length (L). Since this value ranges between 0 and 1, it allows distinguishing how much the trajectory deviates from a linear motion (D/L = 1). Thus, this value can be used in addition to the curvature as an indication of the enantiomeric excess. As can be seen from Figure S9, the trend of the straightness index values (green line) is in good agreement with the measured curvatures (yellow line), revealing the expected mirror symmetry.

Discussion

We have designed original hybrid polymer objects, allowing the coupling of a BOD enzyme, which reduces oxygen at the air-water interface, with inherently chiral oligomers for the enantioselective oxidation of DOPA as chiral probe molecules. The propulsion mechanism is based on a site-specific proton flux, accompanying the transport of electrons across the swimmer. The average speed of the swimmers is directly correlated with the concentration of the chiral probes in solution, following a Michaelis Menten type kinetics.
The resulting autonomous swimmers show excellent enantioselection abilities, expressed by trajectories that are intimately correlated with the presence of the chiral molecules in solution. Both, the enzyme and the enantiopure oligomers were deposited on a freestanding Ppy film with good mechanical properties and a sufficiently low weight to allow the object to move freely at the air/water

interface. Once placed at the surface of a buffer solution, these swimmers can move clockwise, anticlockwise or straight in a controllable way according to the diastereomeric interactions between the chiral probe and the enantiopure oligomers. The concept has been shown to be of general validity by testing another chiral probe, L-ascorbic acid, having completely different chemical features. Enantioselective macroscopic motion could be observed also in this case. Furthermore, the system is equally operating in serum as a more complex model matrix. This allows imagining further tests with other molecules, additional chiral selectors and different enzymes in follow-up experiments, to further demonstrate the versatility of the presented method. One interesting possible extension could be for example the analysis of the ratio between D- and L-amino acids *via* a selective "on the fly" biodetection.[49] In biology normally the L-form of amino acids is largely dominating, whereas increasing levels of certain D-amino acids have been attributed to different pathologies, such as chronic kidney disease and neurological disorders, like schizophrenia and Alzheimer's disease, as well as an index of bacterial activity in food.[50] Thus, deciphering the ratio between D- and L-amino acids could not only be useful for biomedical aspects, but also as a marker of quality, authenticity, and safety of food, since for example a large content of D-alanine in fruit juice is an indication of high bacterial activity.

On a more general level, one can also imagine using this approach as a very visual and dynamic analogue of a polarimeter. In such measurements, the excess of one enantiomer normally causes rotation of linearly polarized light by a certain angle, which can be detected using dedicated optical equipment. With the swimmers presented here, such a readout would be more straightforward and low-cost, because it is sufficient to observe the trajectory of the swimmer. In addition, downsizing the swimmers with the help of micro- or nanofabrication techniques could open application perspectives where size can be a limitation, such as for detection systems in microfluidic devices.

In conclusion, the common and most important feature is that the macroscopic motion can be modulated by varying the ratio and concentration of the two enantiomers, thus translating enantiomeric excess into different curvatures of the trajectories. This allows a very straightforward and easy macroscopic readout of the chiral information present at the molecular level. Therefore, these chiral bipolar bioelectrocatalytic objects constitute a solid basis for designing a novel family of functional swimmers for which the motion is governed by the chiral character of their environment. Finally, although this work has a pronounced proof-of-concept character, the remarkable behavior of these hybrid swimmers might stimulate the imagination concerning future and eventually totally unexpected applications.

Methods

Macroscopic enantioselective motion experiments.

Experiments with 3,4-dihydroxyphenylalanine (DOPA). The macroscopic motion was recorded by placing the swimmers, prepared according to the procedures described in the supplementary information, at the air/water interface of a 0.3 M citrate/phosphate buffer solution, containing 5mM L-DOPA or 5mM D-DOPA, or the DOPA racemate. A quadratic plastic container, large enough to avoid border effects, has been used for all experiments. The active parts of the swimmer, enzyme and oligomers, were facing the solution. Temperature and pH of the buffer (22°C; pH 5) were optimized to ensure on the one hand the best enzyme activity, but on the other hand to avoid also parasitic effects due to thermal convection.

Experiments with L-ascorbic acid (L-AA). The same operating conditions were used for the experiments carried out L-AA. A 0.25 mM solution was employed for the swimming experiments, and a 1.25 mM solution for DPV recordings.

Experiments with Bovine Serum. The bovine serum (Thermo Fisher Scientific, origin: New Zealand, Gibco, Invitrogen Corporation) was carefully mixed with L-DOPA (10 mM) before filling the container. Macroscopic motion was then recorded at room temperature with swimmers that were prepared according to the procedures described in the supplementary information.

Motion was recorded with a camera (Campark 4K 20MP), having a video resolution of 4K/30fps. Videos were then analyzed using Image J software. The average speed was calculated, in the case of the full circle motion, by dividing the perimeter by the total time needed by the swimmer to browse the full circle.
In the case of straight trajectories, the average speed was calculated with the plug-in Manual Tracking of Image J software.

Proton flux experiments. The swimmers were glued on an inert support, with the active part in contact with the buffer solution containing 5mM of D-DOPA. 1 mm diameter carbon beads were placed in the solution to visualize the hydrodynamic flow triggered by the proton flux. Videos were analyzed with the Image J software, in particular using the z project stack.

Ionic Strength experiments. The experiments were carried out in three buffer solutions at pH 5 with different concentrations: 0.15 M, 0.3 M, 0.5 M. 5 mM D-DOPA was added in all three media. Motion was recorded at room temperature with swimmers that were prepared according to the procedures described in the supplementary information. Videos were analyzed using Image J software. The average speed was calculated by dividing the perimeter by the total time needed by the swimmer to browse the full circle.

Calibration plot experiments. For the study of the variation of average speed with concentration, the polypyrrole film was not cut into two strips, and only one enantiomer, (*S*)-BT_2T_4, was deposited on one extremity of the Ppy. At the other extremity, the hydrogel was drop casted according to the procedure described in the supplementary information. Swimmers were then placed in a 0.3 M citrate/phosphate buffer solution at pH 5, containing L-DOPA in a concentration range from 0.15 mM to 14 mM. For the measures in oxygen or nitrogen saturated solutions, gases were bubbled with a needle through the solution for one hour before placing the swimmer and recording its movement. During the measurement, the container was covered with a transparent plastic cap in order to slow down the gas exchange.

Enantiomeric excess determination. For the enantiomeric excess determination, 0.3 M citrate/phosphate solutions at pH 5 with varying L-DOPA/D-DOPA ratios were prepared. The total concentration of L + D-DOPA was kept constant at a value of 5 mM in all cases. Seven solutions with the following L-DOPA/D-DOPA ratios were tested: 90:10, 70:30, 60:40, 50:50, 30:70, 40:60, 10:90. Experiments were also performed at a lower total concentration of 2.5 mM for the L-DOPA/D-DOPA ratios of 90:10, 60:40, 50:50, 40:60, 10:90. Videos were analyzed with Image J software, in particular by using the z project stack. Curvatures of the trajectories were calculated by drawing a circle fitting the curvature at the maximum point of curling. The radius of the circle was measured and the curvature was

calculated as the reciprocal of the radius. As an alternative, the straightness index was estimated by measuring the distance between the endpoint and the starting point of the trajectory and dividing it by the total length of the trajectory.

SEM and Energy-dispersive X-ray spectroscopy (EDS). SEM experiments together with EDS mapping were carried out using a Vega3 Tescan 20.0 kV microscope.

References

1. Paxton, W. F., Sundarajan, S., Mallouk, T. E. & Sen, A. Chemical locomotion. *Angew. Chem., Int. Ed.* **45**, 5420–5429 (2006).
2. Sengupta, S., Ibele, M. E. & Sen, A. Fantastic Voyage: Designing self-powered nanorobots. *Angew. Chem. Int. Ed.* **51**, 8434–8445 (2012).
3. Pacheco, M., Lopez, M. A., Jurado-Sanchez, B. & Escarpa, A. Self-propelled micromachines for analytical sensing: a critical review. *Anal. Bioanal. Chem.* **411**, 6561-6573 (2019).
4. Sheng Moo, J. G., Mayorga-Martinez, C. C., Wang, H., Khezri, B., Teo, W. Z. & Pumera, M. Nano/Microrobots meet electrochemistry. *Adv. Funct. Mater.* **27**, 1604759 (2017).
5. Kong, L., Guan, J. & Pumera, M. Micro- and nanorobots based sensing and biosensing. *Curr. Opin. Electrochem.* **10**, 174–182 (2018).
6. Campuzano, S., Esteban-Fernández De Ávila, B., Yáñez-Sedeño, P., Pingarrón, J. M. & Wang, J. Nano/microvehicles for efficient delivery and (bio)sensing at the cellular level. *Chem. Sci.* **8**, 6750–6763 (2017).
7. Duan, W., Wang, W., Das, S., Yadav,V., Mallouk, T. E. & Sen, A. Synthetic Nano- and Micromachines in Analytical Chemistry: Sensing, Migration, Capture, Delivery, and Separation. *Annu. Rev. Anal. Chem.* **8**, 311–333 (2015).
8. Ismagilov, R. F., Schwartz, A., Bowden, N. & Whitesides, G. M. Autonomous movement and self-assembly. *Angew. Chemie - Int. Ed.* **41**, 652–654 (2002).
9. Ozin, G. A., Manners, I., Fournier-Bidoz, S. & Arsenault, A. Dream nanomachines. *Adv. Mater.* **17**, 3011–3018 (2005).
10. Sanchez, S., Soler, L. & Katuri, J. Chemically powered micro- and nanomotors. *Angew. Chemie - Int. Ed.* **54**, 1414–1444 (2015).
11. Turner, L., Ryu, W. S. & Berg, H. C. Real-Time imaging of fluorescent flagellar filaments. *J. Bacteoriol. Res*. **182**, 2793–2801 (2000).
12. Darnton, N. C., Turner, L., Rojevsky, S. & Berg, H. C. On torque and tumbling in swimming Escherichia coli. *J. Bacteriol*. **189**, 1756–1764 (2007).
13. Magdanz, V., Sanchez, S. & Schmidt, G. Development of a sperm-flagella driven micro-bio-robot. *Adv. Mater*. **25**, 6581–6588 (2013).
14. Hess, H. & Bachand, G. D. Biomolecular motors. *Mater. Today* **8**,

22–29 (2005).
15. Xu, H., Medina-Sanchez, M. & Schmidt, O. G. Magnetic micromotors for multiple motile sperm cell capture, transport, and enzymatic release. *Angew. Chemie - Int. Ed.* **59**, 15029–15037 (2020).
16. Schmidt, C. K., Medina-Sanchez, M., Edmondson, R. J. & Schmidt O. G. Engineering microrobots for targeted cancer therapies from a medical perspective. *Nat. Comm.* **11**, 5618 (2020).
17. Wu, J., Balasubramanian, S., Kagan, D., Manian Manesh, K., Campuzano, S. & Wang, J. Motion-based DNA detection using catalytic nanomotors, *Nat. Comm.* **1**, 36 (2010).
18. Wang, J. Nanomachines: Fundamentals and Applications, Wiley-VCH, (2013).
19. Sun, J., Mathesh, M., Li, W. & Wilson, D. A. Enzyme-powered nanomotors with controlled size for biomedical applications. *ACS Nano* **13**, 10191–10200 (2019).
20. Mathesh, M., Sun, J. & Wilson, D. A. Enzyme catalysis powered micro/nanomotors for biomedical applications. *J. Mater. Chem. B* **8**, 7319–7334 (2020)
21. Yuan, H., Liu, X., Wang, L., Ma, X. Fundamentals and applications of enzyme powered micro/nano-motors. *Bioact. Mater.* **6**, 1727–1749 (2021).
22. Dey, K. K., Zhao, X., Tansi, B. M., Mendez-Ortiz, W. J., Cordova-Figueroa, U. M., Golestanian, R. & Sen, A. Micromotors powered by enzyme catalysis. *Nano. Lett.* **15**, 8311-8315 (2015).
23. Pavan Kumar, B. V. V. S., Patil, A. J. & Mann, S. Enzyme-powered motility in buoyant organoclay/DNA protocells. *Nat. Chem.* **10**, 1154-1163 (2018).
24. Soong, R. K., Bachand, G. D., Neves, H. P., Olkhovets, A. G., Craighead, H. G. & Montemagno, C. D., Powering an inorganic nanodevice with a biomolecular motor. *Science.* **290**, 1555–1558 (2000).
25. Mano, N. & Heller, A. Bioelectrochemical propulsion. *J. Am. Chem. Soc.* **127**, 11574–11575 (2005).
26. Pantarotto, D., Browne, W. R. & Feringa, B. L. Autonomous propulsion of carbon nanotubes powered by a multienzyme ensemble. *Chem. Commun.* 1533–1535 (2008).
27. Sanchez, S., Solovev, A. A., Mei, Y. F. & Schmidt, O. G. Dynamics of biocatalytic microengines mediated by variable friction control. *J. Am. Chem. Soc.* **132**, 13144–13145 (2010).
28. Orozco, J., García-Gradilla, V., D'Agostino, M., Gao, W., Cortés, A. & Wang, J. Artificial enzyme-powered microfish for water-quality testing. *ACS Nano* **7**, 818–824 (2013).
29. Simmchen, J., Baeza, A., Ruiz, D., Esplandiu, M. J. & Vallet-Regí, M. Asymmetric hybrid silica nanomotors for capture and cargo transport: Towards a novel motion-based DNA sensor. *Small* **8**, 2053–2059 (2012).

30. Zhao, G., Sanchez, S., Schmidt, O. G. & Pumera, M. Poisoning of bubble propelled catalytic micromotors: The chemical environment matters. *Nanoscale* **5**, 2909–2914 (2013).
31. Villa, K., Manzanares Palenzuela, C. L., Sofer, Z., Matějková, S. & Pumera, M. Metal-Free Visible-Light Photoactivated C3 N4 Bubble-Propelled Tubular Micromotors with Inherent Fluorescence and On/Off Capabilities. *ACS Nano* **12**, 12482–12491 (2018).
32. Wang, K.,Wang, W., Pan, S., Fu, Y., Dong, B. & Wang, H. Fluorescent self-propelled covalent organic framework as a microsensor for nitro explosive detection. *Appl. Mater. Today* **19**, 100550 (2020).
33. Iamsaard, S., Aßhoff, S. J., Matt, B., Kudernac T., Cornelissen, J. J. L. M., Fletcher, S. P. & Katsonis, N. Conversion of light into macroscopic helical motion. *Nat. Chem.* **6**, 229–235 (2014).
34. Lee, K. M., Smith, L. M., Koerner, H., Tabiryan, N., Vaia, R. A., Bunning, T. J. & White, T. J. Photodriven, flexural-torsional oscillation of glassy azobenzene liquid crystal polymer networks. *Adv. Funct. Mater.* **21**, 2913–2918 (2011).
35. Arnaboldi, S., Grecchi, S., Magni, M. & Mussini, P. Electroactive chiral oligo- and polymer layers for electrochemical enantiorecognition. *Curr. Opin. Electrochem.* **7**, 188–199 (2018).
36. Arnaboldi, S., Gupta, B., Benincori, T., Bonetti, G., Cirilli, R. & Kuhn, A. Absolute Chiral Recognition with Hybrid Wireless Electrochemical Actuators. *Anal. Chem.* **92**, 10042–10047 (2020).
37. Sengupta, S., Patra, D., Ortiz-Rivera, I., Agrawal, A., Shklyaev, S., Dey, K. K. Cordova-Figueroa, U., Mallouk, T. E. & Sen, A. Self-powered enzyme micropumps. *Nat. Chem*. **6**, 415–422 (2014).
38. Gupta, B., Afonso, M. C., Zhang, L., Ayela, C., Garrigue, P., Goudeau, B. & Kuhn, A. Wireless Coupling of Conducting Polymer Actuators with Light Emission. *ChemPhysChem* **20**, 941–945 (2019).
39. Gupta, B., Goudeau, B., Garrigue, P. & Kuhn, A. Bipolar Conducting Polymer Crawlers Based on Triple Symmetry Breaking. *Adv. Funct. Mater.* **28**, 1–6 (2018).
40. Gupta, B., Goudeau, B. & Kuhn, A. Wireless Electrochemical Actuation of Conducting Polymers. *Angew. Chemie - Int. Ed.* **56**, 14183–14186 (2017).
41. Mano, N. & de Poulpiquet, A. O_2 reduction in enzymatic biofuel cells. *Chem. Rev*. **118**, 2392-2468 (2018).
42. Paxton, W. F., Kistler, K. C., Olmeda, C. C., Sen, A., St. Angelo, S. K. Cao, Y., Mallouk, T. E., Lammert, P. E. & Crespi, V. H. Catalytic nanomotors: autonomous movement of striped nanorods. *J. Am. Chem. Soc.* **126**, 13424–13431 (2004).
43. Brooks, A. M., Tasinkevych, M., Sabrina, S., Velegol, D., Sen, A. & Bishop, K. J. M. Shaped-directed rotation of homogeneous micromotors

via catalytic self-electrophoresis. *Nat. Comm*. **10**, 495 (2019).
44. Zhan, X., Wang, J., Xiong, Z., Zhang, X., Zhou, Y., Zheng, J., Chen, J., Feng, S.-P. & Tang, J. Enhanced ion tolerance of electrokinetic locomotion in polyelectrolyte-coated microswimmer. *Nat. Comm*. **10**, 3921 (2019).
45. Williams, B. J., Anand, S. V., Rajagopalan, J. & Saif, M. T. A. A self-propelled biohybrid swimmer at low Reynolds number, *Nat. Comm.* **5**, 3081 (2014).
46. Moran, J. & Posner, J. Microswimmer with no moving parts. *Phys. Today* **72**, 44–50 (2019).
47. Hamilton, J. J., Bryan, M. T., Gilbert, A. D., Ogrin, F. Y. & Myers, T. O. A new class of magnetically actuated pumps and valves for microfluidic applications. *Sci. Rep*. **8**, 933 (2018).
48. Mano, N., Kim, H. H., Zhang, Y. & Heller, A. An oxygen cathode operating in a physiological solution. *J. Am. Chem. Soc*. **124**, 6480-6486 (2002).
49. García-Carmona, L., Moreno-Guzmán, M., González, M. C. & Escarpa A., Class enzyme-based motors for"on the fly"enantiomer analysis of aminoacids. *Biosens. Bioelectron.* **96**, 275-280 (2017).
50. Rosini, E., D'Antona, P. & Pollegioni, L., Biosensors for D-Amino Acids: Detection Methods and Applications. *Int. J. Mol. Sci.* **21**, 4574 (2020)

Acknowledgments
The work has been funded by the European Research Council (ERC) under the European Union's Horizon 2020 research and innovation program (grant agreement n° 741251, ERC Advanced grant ELECTRA). S.A. acknowledges financial support of Università degli Studi di Milano for a partial post-doc scholarship. The authors are also very grateful for fruitful discussions with Patrizia Mussini.

Author contributions
S.A. performed the experiments, wrote and edited the manuscript. G.S. performed experiments, wrote and edited the manuscript and treated the data. S.A and G.S contributed equally. A.K. performed enzyme characterization and immobilization experiments. P.G. assisted with electron microscopy characterization. T.B. designed the inherently chiral monomers and edited the manuscript. G.B. synthesized the BT_2-T_4 molecules. R.C separated the

enantiomers by chiral HPLC. S.B. synthesized the redox polymer and tested the BOD under heterogeneous conditions. S.G produced, purified, and tested the BOD in homogeneous solution. N.M. discussed the results and edited the manuscript. A.Ku. proposed the research project, provided resources, designed the experiments, and edited the manuscript.

Data Availability

The datasets generated and analysed in the frame of the current study are available from the corresponding author on request.

Competing financial interests

The authors declare no competing financial interests.